A comparison of computational and experimental methods for determining the gas-flow patterns in the kraft recovery boiler

A. K. Jones* **and T. M. Grace**
The Institute of Paper Chemistry, Appleton, Wis. 54912

J. E. Monacelli
Babcock & Wilcox, Power Generation Group, Barberton, Ohio 44203

ABSTRACT *Computational fluid dynamics was applied to the problem of gas flow in the kraft recovery furnace. For simplicity, the case chosen to be modeled was a cold-flow case, which focuses on flow patterns that derive directly from the method of air introduction and furnace geometry while ignoring the effects of combustion, temperature distribution, and interactions with sprayed liquor. The framework for the model was a commercially available, finite-difference, computational fluid-flow program. A three-dimensional description of the recovery furnace was obtained using 50,000 computational cells. Bilateral symmetry of the furnace was assumed to reduce the computational effort by a factor of two. The results of the computational model are compared with experimental cold-flow data obtained on a 1/8th-scale model of a recovery furnace. The analytical model corresponded closely with cold-flow data obtained experimentally.*

KEYWORDS
Fluid flow
Gas flow
Mathematical models
Recovery furnaces
Simulation

This article describes the first stage in the development of a three-dimensional mathematical model of a recovery furnace. This stage involved simulating cold flow in an existing furnace design. In a cold-flow model, the gas-flow pattern is assumed to be affected only by the geometry of the furnace and the method of air introduction. The effects of temperature, combustion, and the interaction between the black-liquor spray and the gas phase are ignored.

The mathematical model is based on a B&W recovery furnace in a Louisiana mill. This particular furnace was chosen because the manufacturer already had conducted cold-flow tests on a 1/8th-scale model of this furnace. The results from these tests included velocity profiles that were used as a basis of comparison for the simulated results.[1]

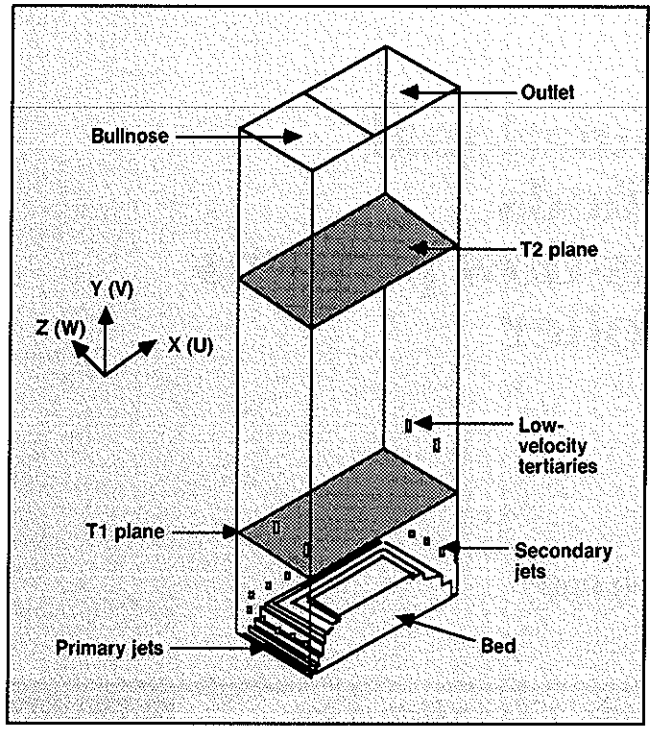
Two computationally developed gas-flow patterns are presented here and compared with two flow patterns that were derived experimentally from the scale model of the B&W recovery furnace. The mathematically derived flow patterns were obtained using a commercially available, computational fluid-flow program known as Fluent.

The computational flow fields were obtained from an analytical cold-flow model of the boiler at 273 K. The experimental flow fields were developed by the manufacturer in a scale model of the same recovery furnace. The manufacturer's report provides scaling constants for converting the velocities up to the full-sized furnace at 477 K. These velocities were then corrected to 273 K for comparison with the computational results.

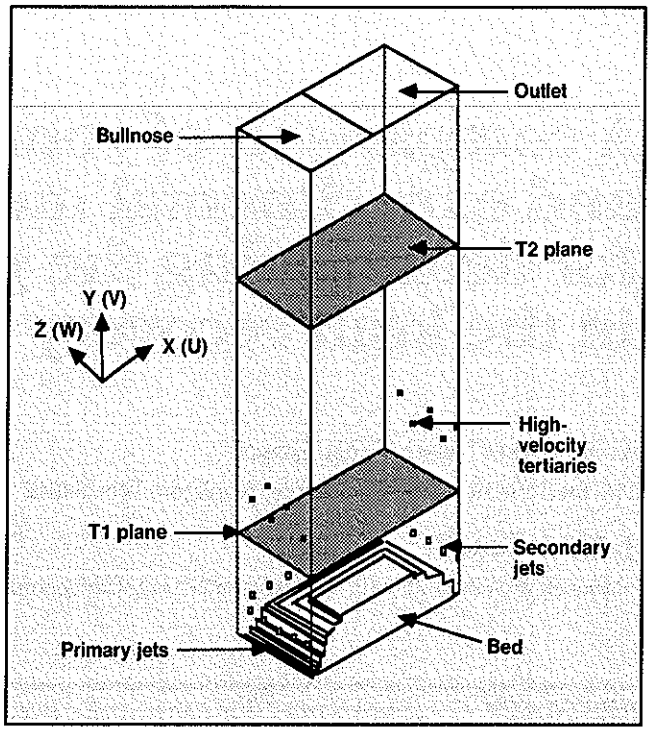
*Jones currently works for Combustion Engineering, 99 Banks Street, Ottawa, Ont., Canada K1P 6C5

[1]Dykshoorn, P., Process Recovery Boiler Flow Model Tests, RDD:87:6940-01-01:01, Babcock & Wilcox, Barberton, Ohio, July 1986.

1. Furnace geometry with low-velocity tertiaries



2. Furnace geometry with high-velocity tertiaries

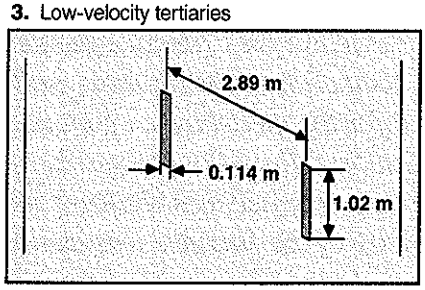


Fluid-flow program

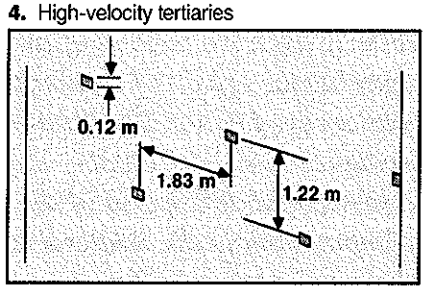
The main tool used in the computational simulation was Fluent, a finite-difference program for modeling fluid flows. This program is flexible and comprehensive, permitting its use in a wide variety of flow situations, including two- or three-dimensional flows, laminar or turbulent flows, and swirling flows. Additional features of Fluent include a six-flux radiation model, the PSI-CELL model for two-phase flow,[2] a combustion model, a number of turbulence models, and a porous-flow model.

The variables that are solved for in the simplest three-dimensional case are the velocities in the x, y, and z directions (U-velocity, V-velocity, and W-velocity, respectively) and pressure. If temperature effects are added, the enthalpy and the radiative heat fluxes are also determined. If the K-E turbulence model is used, then the kinetic energy of turbulence and the dissipation rate are found. If combustion is included, the mole fractions of combustibles (F), oxygen (O), and products (C) must be calculated in each cell. The maximum number of finite-element cells that can be solved for in the version of Fluent used here (version 2.8) is 50,000.

3. Low-velocity tertiaries



4. High-velocity tertiaries



The attractive features of Fluent include:

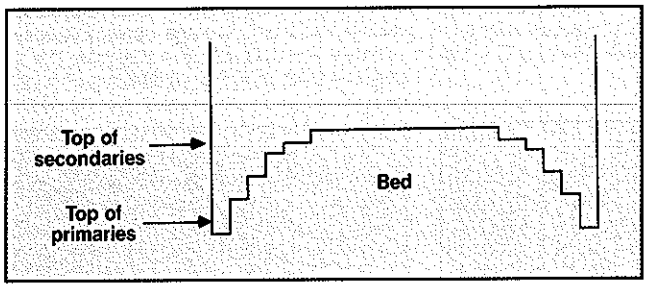
- Interactive input
- Flexibility to model almost any type of flow
- Internally generated relaxation coefficients, which usually result in stable iterations
- Excellent graphics for viewing the results.

The description of a flow is menu driven, so the process of setting up a fluid-flow simulation is straightforward. Either Cartesian or cylindrical regions can be described. In a Cartesian description, the cells are rectangular parallelepipeds that can be different lengths in each coordinate direction. A number of different cell types can be specified. Typically, five different types are used:

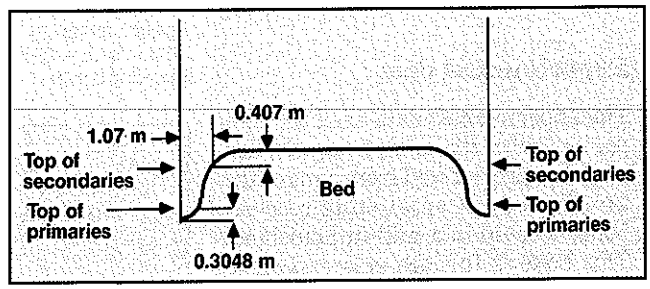
1. Live cells—the variables in these cells are solved for at each iteration
2. Inlet cells—the values of the flow variables are specified for these cells and remain the same throughout the calculation
3. Wall cells—these cells act as barriers to the flow and are used to describe the flow geometry
4. Outlet cells—values for the flow variables are solved for, but these cells are placed on boundaries of the flow
5. Symmetry cells—these cells define lines or planes of symmetry in the flow, which reduces the number of cells necessary to describe a given flow geometry.

[2]Crowe, C. T. and Sharma, M. P., J. Fluids Eng. 99(6): 325(1977).

5. Outline of computational bed



6. Dimensions of experimental bed



In addition to a description of the flow geometry, it is necessary to specify the physical properties of the fluid and the boundary conditions in the wall and inlet cells. The mass flow rates in the inlet cells are controlled by varying the gas velocity or the distance between adjacent nodes.

The cold-flow simulation

The analytical cold-flow model was set up with physical dimensions as close as possible to those of the full-sized furnace to justify comparison between the experimental and analytical cases. Some approximation was necessary because of the upper limit of 50,000 nodes. An isoparametric view of the furnace is shown in **Figs. 1 and 2.** Because of the bilateral symmetry involved, it is only necessary to describe half of the furnace. The flow patterns in the other half of the furnace are a mirror image of the modeled area of the furnace. The symmetry plane is parallel to the side walls and bisects the bullnose and the bed.

The full-sized furnace is 9.6 m × 10.6 m in cross section and 27.0 m high (to the bullnose). The computational model is 10.0 m × 5.0 m and 30.0 m high. (The cross section of the model is approximately half that of the full-sized furnace because of the presumed bilateral symmetry.) The bullnose extends 5 m across the top of the furnace in both cases. The actual bullnose slopes slightly downward to the back of the furnace, but this was ignored in the computational model in order to reduce the number of nodes used. The resulting effect on the gas-flow patterns should be negligible, as the slope is minimal.

The primary, secondary, and tertiary air inlets were modeled in the following manner.

Primary air

A row of nodes along the walls were designated as primary air inlets. The distances between the inlet nodes and the nodes above and below were adjusted to satisfy the volumetric flow rates. This treats the primary air as a planar jet completely encircling the furnace. A shortage of nodes made description of individual primary ports impractical. The primary air was injected 1 m above the furnace floor at a velocity of 40 m/s.

Secondary air

The individual secondary air ports in the model were of approximately the same dimensions as the ports in the actual furnace. The dimensions of the ports in the full-sized furnace were 7.6 cm × 35.5 cm. In the model, they were 11.4 cm × 23.7 cm. The areas were the same, but the individual dimensions had to be adjusted. This approximation was necessary to accommodate computer hardware limitations, which restricted the total number of cells that could be used. The 11.4-cm width of the secondary and tertiary air ports was an average of the actual widths. The modeled half of the furnace had 16 secondary ports, each with an inlet velocity of 36 m/s (identical to the prototype furnace). The injection level was 3 m above the furnace floor.

Tertiary air

The separate tertiary air ports on the walls of the model were of approximately the same shape as those in the actual furnace. Two configurations were examined, creating two computational cases. The computational cases were set up so that they corresponded as closely as possible to the two experimental cases.

In the first configuration, four ports were placed 10 m above the furnace floor, with two ports on the front wall and two on the back wall, as seen in Fig. 1. These low-velocity ports had an inlet velocity of 10 m/s (identical to the prototype furnace). A close-up view of the ports is provided in **Fig. 3.** The port sizes were 11.4 cm × 1.02 m, the same area as the actual ports, which were 15.2 cm × 76.2 cm.

In the second configuration, eight smaller ports with an inlet velocity of 77 m/s were used, with four ports on the front wall and four on the back wall. Two closely spaced levels of tertiary air were used (at 9.5 m and 10.5 m above the floor of the furnace). A close-up view of the high-velocity ports is provided in **Fig. 4.** The port sizes were 11.4 cm^2, as opposed to the circular 12.7-cm-ID ports used in the actual furnace.

The first configuration corresponded to experimental Case 1, which involved the use of low-velocity tertiaries. The second configuration corresponded to experimental Case 2, which involved the use of high-velocity tertiaries.

The bed shape used in the computational cases is depicted in **Fig. 5.** This shape corresponded as closely as possible to the bed shape used in the experimental work, which is depicted in **Fig. 6.** In both cases, the top of the bed extended slightly above the secondary air ports. The use of body-fitted coordinates would eliminate the staggered bed shape and the resulting numerical problems, leading to a more accurate description of the flow around the bed. However, this is not yet available as part of the Fluent program.

The mass flow rates in the Fluent models were the same as those of the full-sized B&W furnace. The total flow rate for the half of the furnace modeled was 48 kg/s (380,000 lb/h). In Case 1, the flow was split into 50% primary, 40% secondary, and 10% tertiary air. In Case 2, the flow was

split into 46% primary, 36% secondary, and 18% tertiary air.

Experimental data

The experimental data used for comparison with the analytical cold-flow models were derived from a manufacturer's study of an existing recovery boiler located in a mill in Louisiana.[1] This boiler's furnace was experiencing excessive particulate carryover. The problem was believed to be the result of the inability of the existing tertiary air jets to sufficiently break up a high-velocity core of gas.

A variety of changes in the tertiary air system were proposed. These changes were evaluated by constructing a 1/8th-scale replica of the actual recovery furnace and then conducting cold-flow measurements in the replica. The velocities within the scaled-down furnace were measured with a hot-film anemometer at two traverse planes:

- T1, located halfway between the secondary and tertiary air ports
- T2, located about halfway between the tertiary air ports and the bullnose.

Isovelocity plots were constructed using data obtained at these traverse planes.

The two cases that were simulated are designated Case 1 (low-velocity tertiaries) and Case 2 (high-velocity tertiaries). In both cases, a bed was included in the bottom of the furnace.

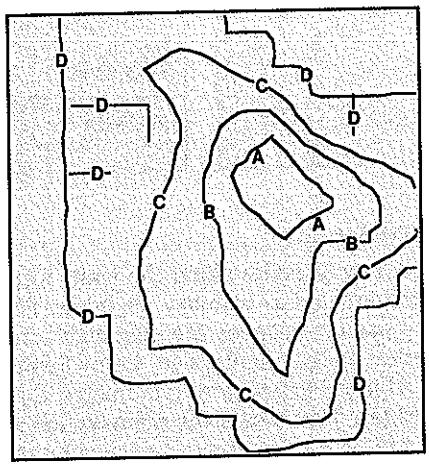
Comparison of experimental and computational cases

The results obtained by modeling experimental Cases 1 and 2 with Fluent were compared on the basis of average upward velocity at 273 K and on the general flow pattern. However, before comparing the experimental and computational cases, it was first necessary to put them on an equal basis.

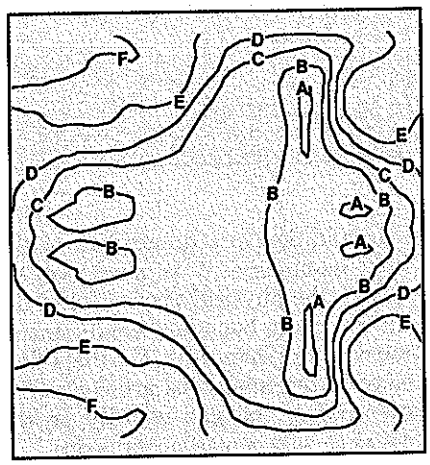
In the experimental work, the average upward velocity was calculated by totaling the different values for positive velocity and then dividing this total by the number of positive velocities. The average upward velocity in the prototype (full-size furnace at 400°F) can then be calculated based on the scaling criteria.

In Case 1, the scaling factor is 218; in Case 2, it is 295. This results in an average velocity in feet per minute, which can then be converted to meters per second. Finally, a temperature correction is applied, converting the experimental results to 273 K. The results obtained computationally are already in units of meters per second at the cold-flow temperature of 273 K.

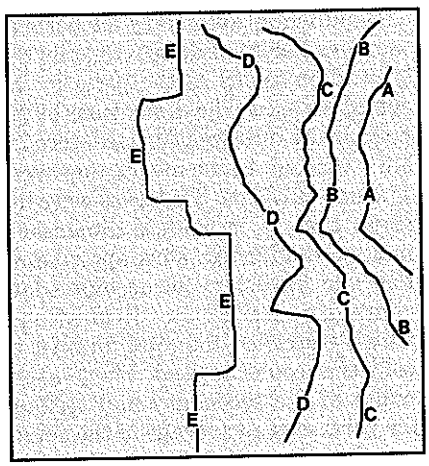
7. Experimental results showing contours of the upward velocity at the T1 slice (Case 1, low-velocity tertiaries). Average upward velocity = 2.38 m/s. A = 4.34 m/s; B = 2.89 m/s; C = 1.45 m/s; D = 0 m/s.



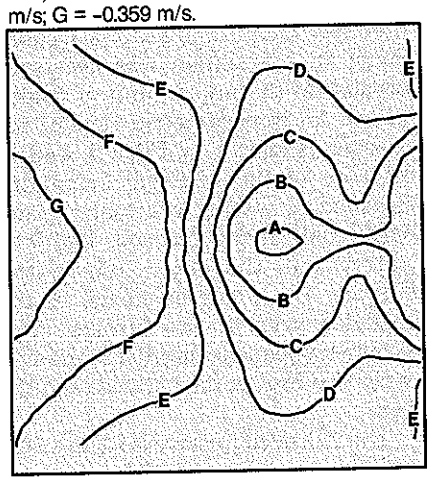
8. Computational results showing contours of the upward velocity at the T1 slice (Case 1, low-velocity tertiaries). Average upward velocity = 1.80 m/s. A = 3.33 m/s; B = 2.26 m/s; C = 1.19 m/s; D = 0.111 m/s; E = -0.964 m/s; F = -2.04 m/s.



9. Experimental results showing contours of the upward velocity at the T2 slice (Case 1, low-velocity tertiaries). Average upward velocity = 1.50 m/s. A = 2.89 m/s; B = 2.17 m/s; C = 1.44 m/s; D = 0.72 m/s; E = 0 m/s.



10. Computational results showing contours of the upward velocity at the T2 slice (Case 1, low-velocity tertiaries). Average upward velocity = 0.83 m/s. A = 2.06 m/s; B = 1.66 m/s; C = 1.25 m/s; D = 0.850 m/s; E = 0.447 m/s; F = 0.044 m/s; G = -0.359 m/s.



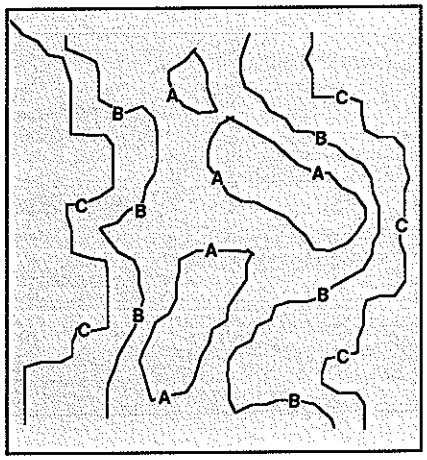
Case 1—low-velocity tertiaries

T1 traverse. The T1 traverse, a horizontal slice located above the bed, is shown in Fig. 1. The experimental and computational contours of the upward velocity (V-velocity) at the T1 slice are shown in **Figs. 7 and 8**, respectively.

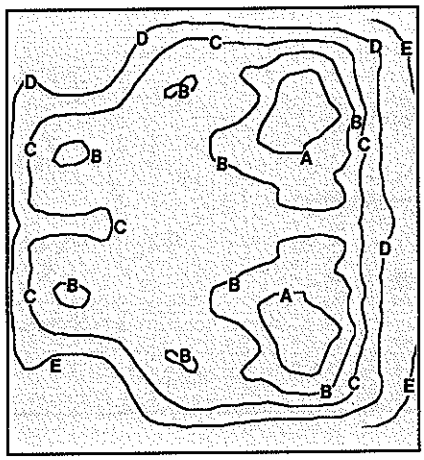
The main features of these contour plots are the upflow region in the center of the furnace and the downflow regions around the outside. The computational T1 traverse for Case 1 shows good agreement with the experimental results with respect to the general flow patterns. The location of downflow regions and the maximum upward velocity correspond to the experimental results.

The average upward velocity is about 40% higher in the experimental case than in the computational case (2.4 m/s vs. 1.8 m/s). This is due to the

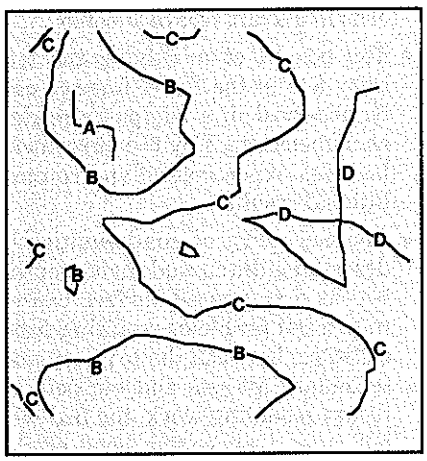
11. Experimental results showing contours of the upward velocity at the T1 slice (Case 2, high-velocity tertiaries). Average upward velocity = 1.92 m/s. A = 3.90 m/s; B = 1.95 m/s; C = 0 m/s.



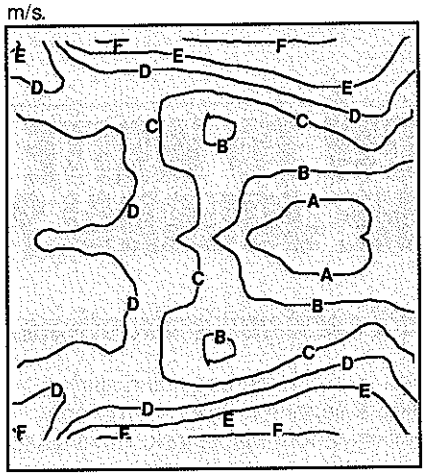
12. Computational results showing contours of the upward velocity at the T1 slice (Case 2, high-velocity tertiaries). Average upward velocity = 1.60 m/s. A = 2.90 m/s; B = 1.72 m/s; C = 0.551 m/s; D = -0.622 m/s; E = -1.80 m/s.



13. Experimental results showing contours of the upward velocity at the T2 slice (Case 2, high-velocity tertiaries). Average upward velocity = 0.80 m/s. A = 1.46 m/s; B = 0.98 m/s; C = 0.49 m/s; D = 0.



14. Computational results showing contours of the upward velocity at the T2 slice (Case 2, high-velocity tertiaries). Average upward velocity = 0.80 m/s. A = 1.55 m/s; B = 1.20 m/s; C = 0.845 m/s; D = 0.483 m/s; E = 0.141 m/s; F = -0.211 m/s.



use of a bed with a staggered shape, which tends to deflect the air jets upward rather than following the surface of the bed. This reduces the intensity of the central core, as some of the gas is deflected upward before it reaches the center of the furnace.

The velocities are highest in the center, as all the secondary jets meet at this point and are forced to move upward. The downflow regions around the perimeter of the furnace are created by the entrainment of gas by the secondary jets.

T2 traverse. The T2 traverse, a horizontal slice located above the tertiary jets, is also illustrated in Fig. 1. In this case, the velocity contours obtained experimentally have taken on a much different appearance, as seen in **Fig. 9**. At the front of the furnace, the upward velocities are large. The back of the furnace is a large stagnant region, resulting in poor use of the furnace volume for combustion of the flue gases.

At the T2 traverse in Case 1, the existence of the large stagnant region seen experimentally is confirmed using the computer model, as seen in **Fig. 10**. The location of the maximum upward velocity is at the front wall in both cases. The average upward velocity in the experimental case is 1.50 m/s, compared with 0.83 m/s in the computational case. Once again, this is the result of the numerical problems caused by the use of a bed with a staggered surface. The effects persist up to the T2 traverse.

Case 2—high-velocity tertiaries

T1 traverse. A comparison of computational and experimental results at the T1 traverse for Case 2 is essentially the same as for Case 1, as seen in **Figs. 11 and 12**. In this case, however, the discrepancy in the average upward velocity is higher (1.60 m/s vs. 2.94 m/s).

T2 traverse. Case 2 has much higher-velocity tertiaries than Case 1. The result is better utilization of the furnace volume, as shown in **Fig. 13**. The stagnant region at the back of the furnace has been eliminated.

The experimental results at the T2 traverse in Case 2 show no downflow, while the computational results have only small areas of downflow against the side walls, as seen in **Fig. 14**. The average upward velocity found experimentally and computationally is the same—0.80 m/s. The numerical problems are no longer a factor because the center core has been almost completely eliminated in both the computational and the experimental data. The average upward velocity should be just the total mass flow rate divided by the cross-sectional area times the density. These values are the same for both the experimental and the computational data.

The reason for the elimination of the stagnant region can be seen by comparing contours of the U-velocities at the tertiary air ports for Cases 1 and 2, illustrated in **Figs. 15 and 16**, respectively. These contours were obtained from a horizontal slice that cuts through the midpoint of the tertiary jets. The greater penetration of the high-velocity tertiaries is immediately apparent. This increased penetration effectively breaks up the core of high-velocity gas created in the lower furnace.

Limitations of modeling techniques

There are inherent drawbacks to numerical and experimental scale models. However, both techniques can be effective if their limitations are

kept in mind.

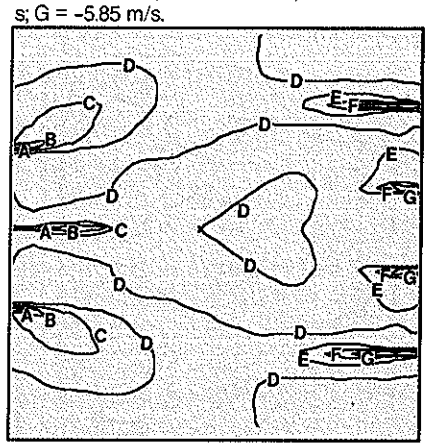
The main limitations of a computer-generated gas-flow model are:

- Use of staggered nodes to describe a diagonal surface (i.e., bed surface)
- Empiricism of built-in turbulence models
- Large amount of computer time required to converge complex problems. (About seven days of CPU time are needed to converge a typical problem on a MicroVax.)
- Difficulty in deciding when a flow pattern has converged
- Limitation in the number of nodes, making it impossible to describe fine details of the flow around the bed and in jets.

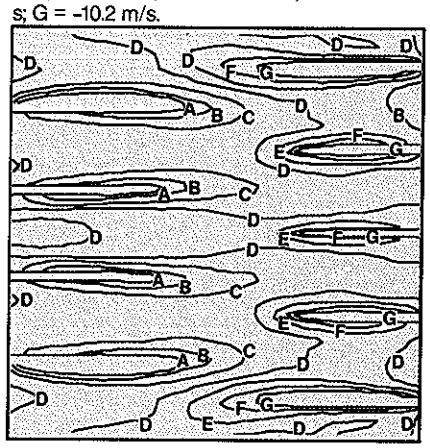
The main limitations of using a scale model to experimentally determine gas flows are:

- Limitation in the extent of changes that can be made once the model has been constructed.
- Difficulty in satisfying all the scaling criteria.
- Difficulty in obtaining numerous velocity measurements, coupled with the fact that the act of measurement may alter velocities.
- Factoring in temperature effects is difficult.

15. Computational results showing contours of the U-velocities at a horizontal slice through the midpoint of the tertiary jets (Case 1, low-velocity tertiaries). A = 5.85 m/s; B = 3.90 m/s; C = 1.95 m/s; D = 0 m/s; E = -1.95 m/s; F = -3.90 m/s; G = -5.85 m/s.



16. Computational results showing contours of the U-velocities at a horizontal slice through the midpoint of the tertiary jets (Case 2, high-velocity tertiaries). A = 10.2 m/s; B = 6.83 m/s; C = 3.41 m/s; D = 0 m/s; E = -3.41 m/s; F = -6.83 m/s; G = -10.2 m/s.



Conclusions

The main conclusions that can be drawn from the modeling effort are:

- A software package (Fluent) can effectively simulate gas-flow patterns in a kraft recovery boiler.
- The benefit of modifying the tertiary jets in the B&W furnace can be observed in a computer model, as demonstrated by the agreement between experimental and computational results.
- The necessity of mathematically describing the curved surface of the bed as a staggered surface causes numerical problems resulting from collisions between the primary and secondary air jets and the bed. In future modeling work, the bed will not extend above the level of the secondaries. This should result in a more realistic flow pattern. □

Portions of this work were used by AKJ as partial fulfillment of the requirements for the Ph.D. degree at The Institute of Paper Chemistry.

WONDERING HOW TO WRITE A PAPER FOR THE JOURNAL?

We'll send you instructions.

When you're in the beginning stages, writing a paper for *Tappi Journal* can seem like a formidable task. There's a lot of information to pull together, and it has to be assembled in a manner that others can understand.

We can't tell you what to write, but we can tell you how to put it together, where to send it and how to give it a better chance of being accepted for publication.

Get started now. Send for our free booklet, "Author Guidelines for Submitting an Article to *Tappi Journal*."

Tappi Journal • Technology Park/Atlanta
P.O. Box 105113 • Atlanta, GA 30348-5113
(404) 446-1400 (ext. 247)